scientific reports

Check for updates

OPEN

Study on hangfire failure mechanism in firearm firing-ignition systems

Shuxia Zhang[1]✉, Yirui Li[2], Zhifang Wei[1], Kebin Zhang[1], Tantao Xiang[1] & Jingguo Liang[1]

To investigate the hangfire failure mechanism in firearm firing-ignition systems, gas pressure responses were experimentally analyzed using a firing-ignition simulation test device. Pressure characteristic parameters were statistically evaluated using the "3σ" criterion to establish the hangfire failure thresholds. A finite element model simulating the mechanical-thermal-chemical multi-mechanism coupling process during primer mixture ignition was developed and validated against experimental results. The effects of percussion energy, interlocking gap, charge surface height, and anvil height on primer mixture temperature and gas pressure dynamics were systematically studied. Single-factor and coupled two-factor analyses revealed critical failure boundaries and their influence on ignition performance. Results indicate that reduced percussion energy and charge surface height, combined with increased interlocking gap and anvil height, diminish energy conversion efficiency, delay hotspot formation, and prolong pressure initiation.

Keywords Firing ignition, Hangfire failure mechanism, Failure boundary analysis, Numerical simulation

The firearm firing-ignition system, responsible for initiating propellant combustion, is prone to hangfire failures due to machining errors, assembly inconsistencies, and prolonged usage. Such failures compromise firearm reliability, risking component damage and operational hazards. Therefore, reducing the failure rate through mechanistic studies is critical for optimizing ignition system design.

Prior studies have extensively researched hangfire failures. Wei et al.[2] investigated the effect of nitrate barium on propellant coating and found that the ignition delay time increased with the rising barium content. Zhang et al.[3] conducted numerical simulations on the two-phase jet firing process of the bottom igniter, analyzing the effects of ignition jet temperature, solid-phase particle diameter, and particle phase concentration on the ignition delay time. Elya Courtney et al.[4] assessed different types of primers under varied environmental conditions and concluded their effects on ignition delay performance. Hu et al.[5] studied the ignition and combustion characteristics of micron aluminum particles and found that increasing the ambient temperature and oxygen content could reduce the ignition delay time of the particles. Li et al.[6] studied the ignition, combustion, and agglomeration characteristics of GAP/CL-20 propellant and found that the ignition delay time and self-sustaining combustion time were shortened when the pressure increased. Several scholars analyzed the impact of different explosive particle diameters on ignition delay[7–9]. Li et al.[10] focused on bore-retained bullets, conducting simulations on percussion energy and the firing pin percussion primer with Adams software and ruling out the possibility of bore-retained bullets due to mechanical firing malfunction. Jing et al.[11] determined the velocity and energy of the firing pin when the firearm was fired reliably through finite element simulation. Ge et al.[12] conducted numerical simulations on the firing process of an automatic rifle and found that firing failure occurred when the blow speed of the hammer was lower than 4.85 m/s. Wang et al.[13] used experimental methods to study the effect of charge density and charge density on the ignition performance of the agent. The experimental results showed that the increase of charge density or charge density would reduce the ignition delay time. Huang[14] simulated the combustion flow process of ignition powder particles during ignition and found that the ignition delay time decreased with the increase of ignition charge. Using Solidworks, Xie et al.[15] addressed bullet retention issues and determined the relative safety time in misfire situations. Wu et al.[16] emphasized bullet retention problems and concluded that delayed ignition occurred when the percussion energy was insufficient under normal conditions. Zhang et al.[17] conducted ballistic mortar tests on a Gatling gun and suggested that hangfire failure might occur under insufficient ignition energy. Courtney M et al.[18] conducted tests on two types of primers and understood that low peak pressure and a large standard deviation led to

[1]College of mechatronic engineering, North University of China, No. 3 Xueyuan Road, Taiyuan 030051, Shanxi Province, PR China. [2]No. 208 Research Institute of China Ordnance Industries, No.57 Ma Xing Road, Nankou, Changping District, Beijing 102202, PR China. ✉email: zhang_shuxia@nuc.edu.cn

delayed ignition. Mei et al.[19] established a virtual prototype model and analyzed the effect of delayed ignition on the dynamic characteristics of internal energy automatics. Zhou et al.[20] created a 3D model of cluster weapons for three-tube in-parallel firing and discovered that hangfire failure led to the deterioration of pellet movement posture and a decline in firing accuracy. Li et al.[21] conducted troubleshooting on a scenario where the shell was ejected outside the chamber of an anti-aircraft gun automatic and found that excessive hangfire failure caused cartridge rupture. Finally, Yang et al.[22] conducted dynamic numerical simulations on the firing process of an automatic and concluded that hangfire failure increased both backlash velocity and resistance. Duan et al.[23] proved that the critical drop hammer height threshold of propellant ignition was 35 cm by experiment and numerical simulation.

Based on the reviewed studies on hangfire failure, the research mainly focuses on the ignition delay of explosive particles and the influence of hangfire failure. There are few studies on the mechanism of percussion energy transfer and conversion into ignition energy, as well as on the relationship between structural parameters such as the interlocking gap, the height of the charge surface, the height of the anvil, and the hangfire failure. Although some literature mentions that insufficient ignition energy will cause hangfire failure, few studies explore the mechanism of ignition energy transfer and conversion. These studies primarily focus on the analysis of single influence factors, while research on the coupling of two factors is limited, and criteria for fault judgment are lacking.

In order to further study the influence mechanism of structural parameters such as percussion energy, interlocking gap, charge surface height, and anvil height on the late firing fault, and to clarify the late firing fault mechanism of the firearm firing-ignition system, this study takes a small-caliber automatic rifle firing-ignition system as an example. Firstly, the firing ignition simulation test device is used to conduct the firing ignition simulation test, and the distribution sample data and probability distribution model of pressure response characteristic parameters are statistically obtained. Based on the '3σ' criterion, the hangfire failure criterion is determined. Then, the finite element simulation model of the firearm ignition process is constructed, and the accuracy of the simulation model is verified by comparing it with the experimental results. Subsequently, focusing on four influence factors: the falling height, interlocking gap, charge surface height, and anvil height, the study uses the temperature response of the primer mixture and gas pressure response in the cartridge cavity as evaluation indexes. Single-factor boundary analyses of hangfire failure are carried out using the control variable method. In scenarios with identical percussion energy, the study applies the optimal Latin hypercube test design to explore the impact of two-factor coupling on the time to pressure initiation, aiming to uncover the mechanism behind hangfire failure. This approach aims to provide a more comprehensive understanding of the factors influencing hangfire failures within the firing system.

Experimental and simulation methods

Firearm firing-ignition simulation test method and failure criterion

To simulate the actual assembly of a firearm firing-ignition system and the firearm firing scenario, a pressure - measured truncated cartridge case with a primer was used as the test object. The cartridge case was placed in the pressure test tooling of the firearm ignition simulation test device[24]. The input energy of the primer was controlled by adjusting the drop height and weight of the drop hammer. The drop hammer freely fell through the guide rail under the influence of gravity and struck the firing pin on the tooling, causing the primer to ignite within the test tooling. During the entire firing process, the gravitational potential energy of the drop hammer was converted into the input energy of the primer and friction work. Ignoring the friction work, it was assumed that the gravitational potential energy of the drop hammer was completely converted into the impact energy of the firing pin hitting the primer.

The calculation formula of gravitational potential energy is as follows:

$$E = mgh \tag{1}$$

Where *m*is the weight of the drop hammer, *h* is the drop height of the drop hammer, and *g* is 9.8 m / s2.The pressure test system in the simulation device was utilized to quantitatively analyze the output pressure of the primer. The assembly structure diagram of the firearm firing-ignition system is presented in Fig. 1. This diagram

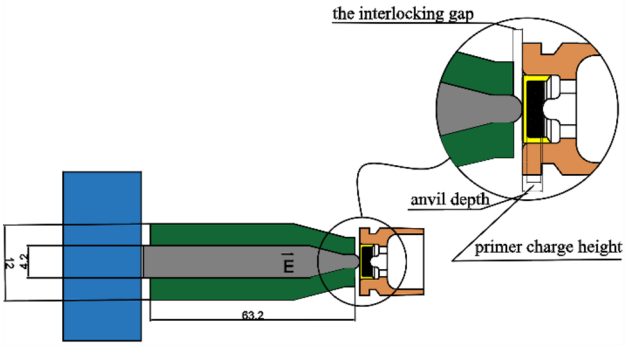

Fig. 1. Assembly structure diagram of firing-ignition system.

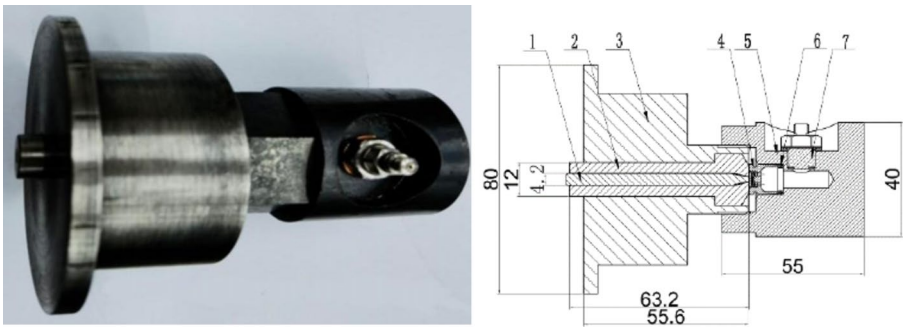

Fig. 2. Truncated casing pressure test kit schematic diagram. 1- Firing pin; 2- Simulated bolt; 3- Installation and positioning tooling; 4- Truncated cartridge case with primer, 5- Sensor mounting block; 6- Washer at the mouth of cartridge case; 7- Piezoelectric pressure sensor.

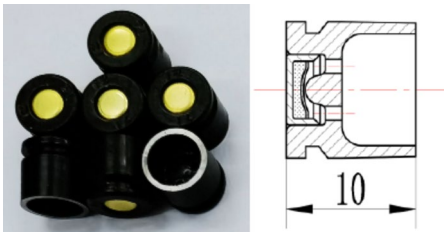

Fig. 3. Pressure-measuring truncated cartridge case with primer.

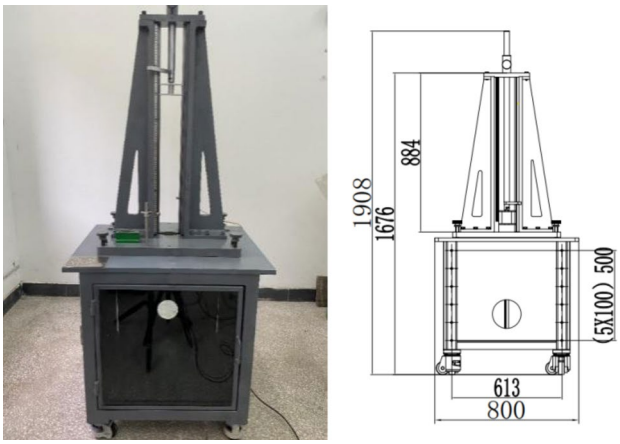

Fig. 4. Firearm firing-ignition simulation experimental device

illustrates the assembly structure of the firearm ignition system and describes its basic composition. The pressure test tooling of the truncated cartridge case is depicted in Fig. 2, and the pressure - measuring truncated cartridge case with primer is shown in Fig. 3. The ignition simulation test device of the firearm is shown in Fig. 4, and the pressure test system is presented in Fig. 5.

Prior to the test, it is essential to level the working table of the firearm ignition system's simulation test device. Subsequently, connect and debug the output gas pressure test system of the firearm ignition system. The detailed debugging procedures are as follows:

a) The piezoelectric pressure sensor is affixed to the pressure - measuring tooling by screwing. Subsequently, one end of the sensor is linked to the charge amplifier, and the sensitivity of the charge amplifier is adjusted to correspond with the parameters of the pressure sensor.
b) Subsequently, link the charge amplifier to the multi - channel data acquisition instrument.
c) Connect the multi-channel data acquisition instrument to the computer;
d) In the dedicated software of the multi - channel acquisition instrument, parameters such as the range and sensitivity of the pressure sensor and acceleration sensor are configured. Additionally, the channel settings,

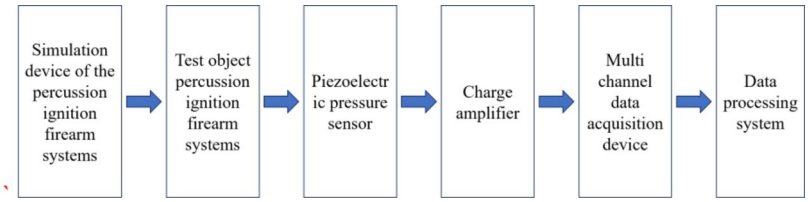

Fig. 5. Test system of gas pressure response

Fig. 6. Piezoelectric pressure transducer.

synchronous trigger settings, as well as parameters like the sampling frequency and sampling time, are completed. Finally, the result file format and path are specified.

After the debugging process is finished, the test steps are as follows:

a) Consult the General specifications for cartridge primer and related information[25]. Use a 250 - g drop hammer to perform the tests at drop hammer heights of 240 mm, 200 mm, and 160 mm. The corresponding percussion energies are 0.588 J, 0.490 J, and 0.392 J respectively. Conduct one group of tests under each test condition, with each group consisting of 10 rounds. In total, 3 groups of 30 rounds will be tested.
b) Insert the sensor gasket into the sensor mounting block and attach the pressure sensor by screwing (after 50 cumulative test rounds, the sensor should be cleaned to minimize errors. Specifically, unscrew the sensor mounting block, remove the pressure sensor, wipe the surface of the pressure sensor with an alcohol - soaked paper towel, clean the sensor mounting hole with a tap, and replace the sensor gasket).
c) Place the bullet sealing washer into the sensor mounting block (when the cumulative number of tests reaches 10, replace it with a new bullet sealing washer), and insert the mouth of the truncated cartridge case with the primer into the sensor mounting block inwards.
d) Position the simulated gun mechanism into the pressure screw and tighten both the pressure screw and the sensor mounting block.
e) Place the test tooling into the tooling mounting hole on the workbench.
f) Insert the firing pin into the simulated gun mechanism.
g) Activate the manual switch on the firearm firing-ignition simulation test device, causing the drop hammer to fall and strike the firing pin, thereby igniting the primer.
h) The pressure data is converted, filtered, amplified, normalized, and modulated by the charge amplifier via the piezoelectric pressure sensor, and is finally acquired and transmitted to the computer. Obtain and save the test data.
i) Unscrew the pressure screw, remove the test truncated cartridge case with the primer, and return to step c) to initiate the next test.
j) To guarantee the accuracy and stability of the test data, repeat the test steps for each working condition 10 times. Calculate the average value of the test data as the test result of the gas pressure response under the firing condition.

Generally, in the free volume of the cartridge case, the gas pressure of the primer output flame of a small - caliber bullet can reach approximately 10 MPa. Consequently, to minimize errors, a piezoelectric pressure sensor with a compatible measurement range should be chosen, as depicted in Fig. 6. The charge amplifier and the data acquisition instrument are presented in Figs. 7 and 8, respectively.

Through data processing, characteristic parameters of the firing-ignition system, such as pressure initiation time, pressure peak, and peak arrival time, are obtained. Figure 9 presents the typical pressure - time response curves under three different percussion energies.

As can be observed from the figure, the pressure start - up time and pressure peak arrival time of the output gas from the firing - ignition system vary significantly depending on the percussion energy. Specifically, the greater the percussion energy, the earlier the pressure start - up time and pressure peak arrival time of the output gas. Scattered data related to pressure characteristic parameters, which are influenced by machining errors, load

Fig. 7. Charge amplifier.

Fig. 8. Data acquisition instrument.

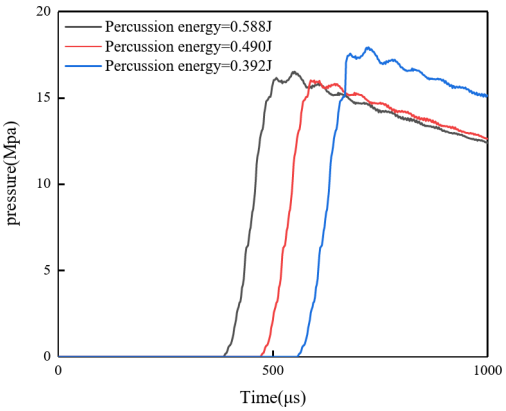

Fig. 9. Primer output pressure-time curve.

errors, and environmental factors, were statistically analyzed. The time to pressure initiation in the gas pressure response output by the firing system was selected as the defining parameter for evaluating firing performance. By using a probabilistic approach, the mean value and standard deviation of the probability distribution model parameters were determined to be 373.29 μs and 59 μs, respectively. Based on the 3σ criterion, the failure criterion for hangfire was set at 550 μs (calculated as $373+3\times59=550$ μs). A hangfire failure is indicated when the time to pressure initiation exceeds 550 μs.

Finite element simulation method of firearm ignition process.

When the primer mixture is subjected to mechanical stimulation, a portion of the mechanical energy is converted into thermal energy through plastic work. This conversion leads to localized thermal accumulation and subsequent hotspot generation[26].

The components within the hotspot undergo thermal decomposition, releasing heat. At this stage, the primer mixture contains both unreacted solid explosive and gaseous reaction products. The JWL equation of state can accurately describe the relationship among parameters such as the density and temperature of detonation products after detonation[27]. Assuming that both the pressure and temperature of the reactant are in an equilibrium state, the two - phase mixture state can be described by the JWL equation, which is expressed as follows:

$$P_s = A_1\left(1-\omega_s/R_1\nu_s\right)\exp^{-R_1\nu_s}+B_1\left(1-\omega_s/R_2\nu_s\right)\exp^{-R_2\nu_s}+\omega_s C_{V\,s}T/\nu_s \tag{2}$$

where the subscript *s* denotes the parameters of unreacted solid explosive, the subscript *g*denotes the parameters of gaseous reaction products, v_s denotes the relative volume of unreacted explosive, *E*denotes the initial internal energy of the solid explosive, C_{Vs}denotes the constant-volume specific heat of unreacted explosive,*E* denotes the average temperature of the explosive mixture, w_s is the Gruneisen coefficient related to the solid, A_1 is the volume compressibility coefficient of the solid, B_1 is the volume correlation coefficient of the solid, R_1 represents the degree of influence of pressure change on the volume change of the solid, and R_2represents the degree of influence of temperature change on the volume change of the solid. The parameters of the state equation can be fitted using the Hugoniot test data.

The pressure of the gaseous reaction product can be defined as:

$$P_g = A_2\left(1-\omega_g/R_3\nu_g\right)\exp^{-R_3\nu_g} + B_2\left(1-\omega_g/R_4\nu_g\right)\exp^{-R_4\nu_g} + \omega_g C_{Vg}T/\nu_g \tag{3}$$

where ν_g denotes the relative volume of gaseous product, C_{Vg} denotes the specific heat of gaseous product,w_g is the Gruneisen coefficient related to the fluid, A_2 is the volume compressibility coefficient of the fluid, B_2 is the volume correlation coefficient of the fluid, R_3represents the degree of influence of pressure change on the volume change of the fluid, and R_4 represents the degree of influence of temperature change on the volume change of the fluid. The parameters of the state equation can be obtained by fitting the cylinder expansion test data.

The chemical reaction occurring within the primer mixture is characterized by the trinomial reaction rate equation[28], which can be expressed as follows:

$$d\lambda/dt = I(1-\lambda)^b(\eta_s-1-a)^x + G_1(1-\lambda)^c\lambda^d p^y + G_2(1-\lambda)^e\lambda^g p^z \tag{4}$$

In this expression, the first term represents the ignition process. It indicates the formation of local explosive hotspots during the impact - compression process and details the subsequent ignition process at these hotspots. The second term accounts for the growth process, describing the localized combustion of the hotspots, specifically the decomposition of unreacted explosive. The third term represents the completion process, depicting the convergence of all hotspots, which enables the rapid conclusion of the reaction within a short period. Where λ denotes the mass fraction of reacted explosives; *t*denotes time, with a unit of μs; $\eta_s$denotes the relative density of unreacted explosives; $\eta_s$denotes the relative density of unreacted explosive; *P*denotes local pressure; *I*and *x* are the number of hot spots, which is a function of shock wave intensity and action time, and *a*is the critical compression degree, that is, when the shock wave is strong enough to act on the explosive so that the compression degree of the explosive is greater than or equal to *a*, the explosion is. The drug ignites. *b* and *c* represent the combustion of inward spherical particles, G_1 and d control the early reaction growth of hot spots after ignition, *y* is the pressure index, and its influence on the model is related to the pressure. G_2, e, g, z determine the reaction rate under high pressure.

The finite element analysis of the firearm firing process was conducted using TrueGrid, LS - DYNA, and LS - PREPOST software. The simulation model was appropriately simplified. Specifically, only the restraining effect of the gun on the firing pin was considered, the hammer was only characterized by its percussion energy, and the shape of the firing pin was assumed to be regular. This model was designed to have the same test conditions, dimensions, and working conditions as the test device.Owing to the axial symmetry of the geometry and impact - loading conditions of the components within the ignition system, a two - dimensional model was adopted. This approach not only reduced the complexity of the solution but also accurately simulated key physical phenomena such as stress - wave propagation and material compression - deformation in the plane. Moreover, in the two - dimensional model, the chemical - reaction rate and the heat - conduction equation could be directly coupled. As a result, it was possible to effectively simulate crucial processes such as hotspot formation and gas - pressure diffusion during the gun - firing ignition process.

Since the unstructured mesh possesses the advantages of superior adaptability to complex geometric shapes, the ability to implement changes in element density, a high degree of automation in the generation method, and robust adaptability, the unstructured form is adopted to construct the mesh model for all components. The 2D simplified model of the firing - ignition system is illustrated in Fig. 10, and the finite - element model of each individual component is depicted in Fig. 11.

To validate the grid sensitivity of the simulation outcomes, four different grid configurations were chosen for verification, with the number of cells being 7909, 7190, 6471, and 5752 respectively. In the course of numerical simulations, the time to pressure initiation at monitoring points was systematically documented. The results of the grid independence analysis are presented in Table 1. The findings reveal that the time to pressure initiation converges when the grid number attains 7190. Thus, after a comprehensive evaluation of computational accuracy and numerical efficiency, the optimal grid configuration consisting of 7190 cells was ultimately selected.

The primer mixture, in which a gas diffusion model was involved, employed the multi - material Arbitrary Lagrange - Euler (ALE) method. For the dispersion of metal components, the Lagrange algorithm was implemented. The trinomial reaction rate equation was utilized to depict the mechano-thermo-chemical response of the propellant under mechanical impact. Based on the ignition growth parameters of C4 explosive, the parameters of the ignition growth state equation were derived, as presented in Tables 2 and 3. The Johnson - Cook constitutive model is capable of taking into account the hardening effect, strain rate effect, and temperature effect of metal materials[29]. The Gruneisen state equation can precisely describe the dynamic behavior of metal materials under high - temperature, high - pressure, and high - strain - rate conditions[30]. The materials of the primer cup, firing pin, and cartridge case were governed by the Johnson - Cook constitutive model and the Gruneisen state equation. The parameters of the state equation are shown in Tables 4 and 5. Furthermore, the bolt, drop hammer, and paper disk adhered to the PLASTIC_KINEMATIC model, with the model parameters

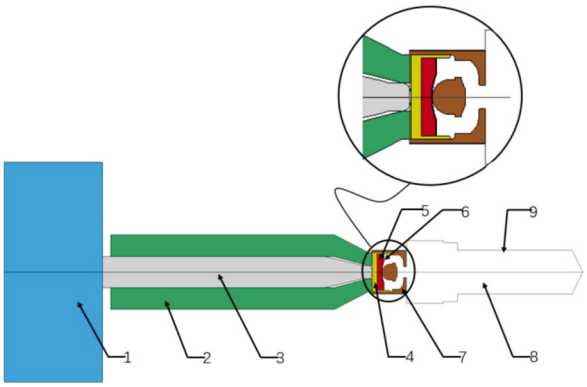

Fig. 10. Simplified finite element model of firing-ignition system. 1- Drop hammer；2- Bolt；3- Firing pin；4- Primer cup；5- Primer mixture；6- Paper disk；7- Cartridge case；8- Air domain 9- Pressure monitoring point

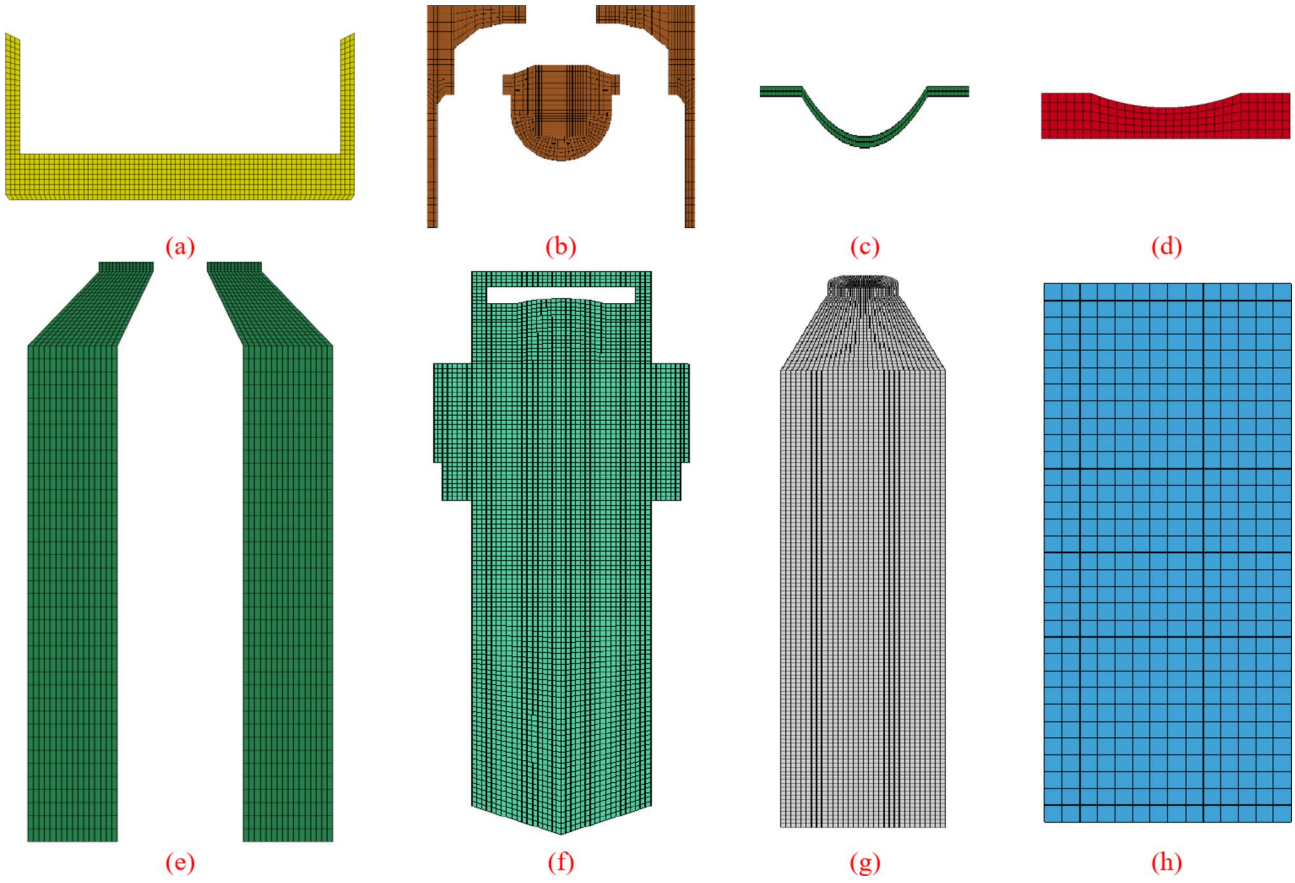

Fig. 11. Finite element model of each component. (**a**) Primer cup, (**b**) Cartridge case, (**c**) Paper disk, (**d**) Primer mixture, (**e**) Bolt, (**f**) Air domain, (**g**) Firing pin, (**h**) Drop hammer

presented in Table 6. The air was modeled using the NULL model. By incorporating material models and parameters for specific components, the accuracy of the simulation model was ensured[24,31].

For structures with relative motion, constraint conditions and contact types were established in accordance with their motion relationships. The boundary conditions and contacts of the model are defined as follows: An initial velocity load is imposed on the hammer to initiate its movement. The side of the cartridge case is subjected to displacement constraints along the direction of the firing - pin movement. A non - reflective boundary condition is applied to the outer region of the air domain.

During the process of the hammer striking the primer cup to ignite the primer mixture, the primer cup experiences significant deformation and may be damaged. Given that the Lagrange algorithm describes material

Number of meshes	Time to pressure initiation/us
7909	392.57
7190	400.00
6471	428.63
5752	504.19

Table 1. Results of mesh sensitivity analysis.

Density (g/cm^3)	Shear modulus (GPa)	Yield stress (MPa)	Hardening modulus	Pressure cut-off valve parameter	Failure strain
2.61	3.36	200	0	-9	1.5

Table 2. Basic parameters of the primer mixture.

A/Mbar	B/Mbar	X_{P1}	X_{P2}	W	R_1	R_2	R_3	R_5	C_{VP}/Mbar·K^{-1}
6.0977	0.1295	4.2	1.1	0.25	778	-0.0503	2.223E-5	11.3	1.0E-5
R_6	A	B	C	d	E	g	I	G_1	C_{VR}/Mbar·K^{-1}
1.13	0.00	0.667	0.667	0.333	0.333	0.667	4000	800	2.78E-5
G_2	X	Y	Z	FMXIG	FMXGR	FMNGR	PCJ/MBar	D/m·s^{-1}	E0/Gerg·mm^{-3}
660	4.0	2.0	3.0	0.30	0.7	0.02	0.3	5200	0.0835

Table 3. Ignition growth state equation parameters of primer mixture.

Parameters	Firing pin	Cartridge case	Primer cup
Density (g/cm^3)	7.85	7.85	8.93
Elastic modulus (MPa)	207	207	110
Shear modulus (GPa)	80	80	40
Poisson ‘s ratio	0.28	0.30	0.32
Yield strength (MPa)	1500	400	190
Strain hardening modulus (MPa)	1770	600	207
Strain hardening factor	0.12	0.26	0.365
Strain rate coefficient	0.016	0.014	0.0376
Thermal softening coefficient	1.25	1.03	1.09
Reference temperature (K)	293	293	293
Quasi-static critical strain rate	1.0	1.0	1.0

Table 4. Johnson-Cook model parameters of primer cup, firing pin and cartridge case.

Material name	Sound velocity (m/s)	Constant coefficient/s	Constant coefficient/$_0$
Firing pin	4569	1.49	2.07
Cartridge case	4569	1.49	2.17
Primer cup	3940	1.92	1.99

Table 5. Mie-Gruneisen equation of state parameters of primer cup, firing pin and cartridge case.

damage through element failure (when the material is destroyed, the element is removed), an erosion model is adopted to define the material of the primer cup. The contact algorithm within the Lagrange algorithm is set as follows:

1) An erosion contact is defined between the primer cup and the firing pin. The static friction coefficient between the two is set at 0.10, and the dynamic friction coefficient is set at 0.01.
2) The primer cup, primer mixture, and paper disk are grouped into a PART set. An automatic single - sided erosion contact is established between each PART within this set. The static friction coefficient is set to 0.3, and the dynamic friction coefficient is set to 0.2.

Parameters	Bolt、drop hammer	Paper disk
Density (g/cm^3)	7.80	1.20
Elastic modulus (MPa)	2.10×10^5	0.6×10^5
Poisson 's ratio	0.30	0.33
Yield stress (MPa)	1000	50
Hardening parameters	1.00	0.00

Table 6. Material parameters of bolt, drop hammer and paper disk.

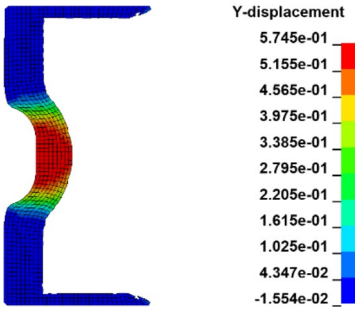

Fig. 12. Pit depth of primer cup.

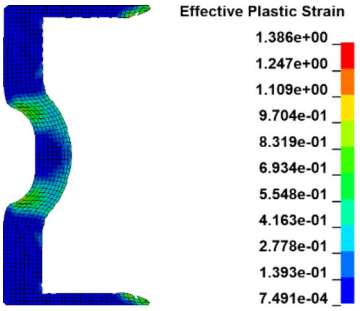

Fig. 13. Stress cloud diagram of primer cup.

3) An erosion contact is defined between the cartridge case and the aforementioned PART set. The static friction coefficient is set at 0.10, and the dynamic friction coefficient is set at 0.01.

For the model employing the fluid - solid coupling algorithm, apart from setting the erosion contacts between the pin - bottom case and the cartridge case - paper cover as described above, it is also essential to define the bottom case and the paper as a PART set and establish the internal PART self - contact. The primer mixture and air are defined as a fluid PART set, and the fluid - solid coupling algorithm is applied between this fluid PART set and the other metal parts.

Simulation result analysis and verification

Analysis of finite element model of firearm firing-ignition process.

The finite - element simulation model of the firing - ignition process was employed to numerically simulate the ignition response behavior of the primer mixture. Specifically, the scenario involved a 250 - g drop hammer striking the firing pin at a velocity of 2.17 m/s (with a percussion energy of 0.588 J). The simulation duration was set to 1000 μs.

The simulation results indicate that the maximum depth of the pit on the primer cup under the impact of the firing pin is 0.575 mm. The displacement contour map and stress contour map of the primer cup at this moment are presented in Figs. 12 and 13, respectively. The stress of the primer mixture reaches its peak around 500 μs, and the corresponding stress contour map is shown in Fig. 14. A local high - temperature region forms around 660 μs, with the temperature reaching 974 K, as depicted in Fig. 15. The entire firing - ignition response process is illustrated in Fig. 16. The primer mixture ignites at 50 μs, and the detonation (combustion) products break through the paper disk and advance towards the fire hole. These products enter the cartridge case via the fire hole at 100 μs, reach the test tool section between 200 μs and 300 μs, and fill the cartridge case and the test tool

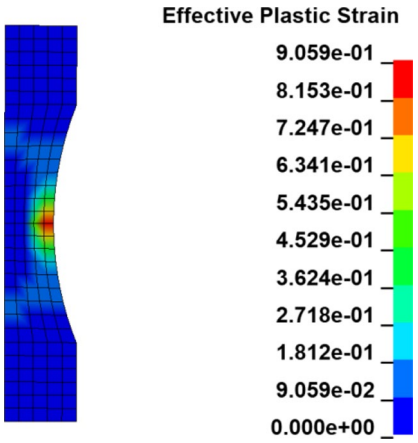

Fig. 14. Stress on primer mixture.

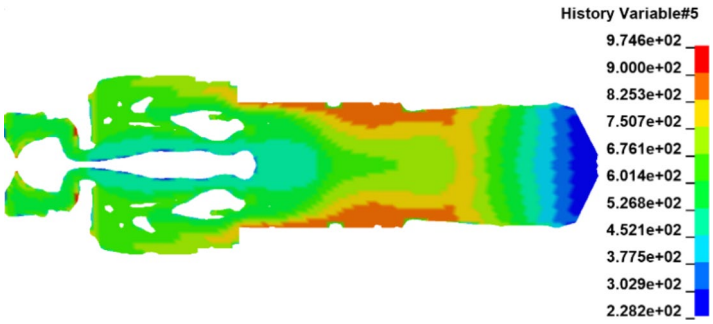

Fig. 15. High gas temperature.

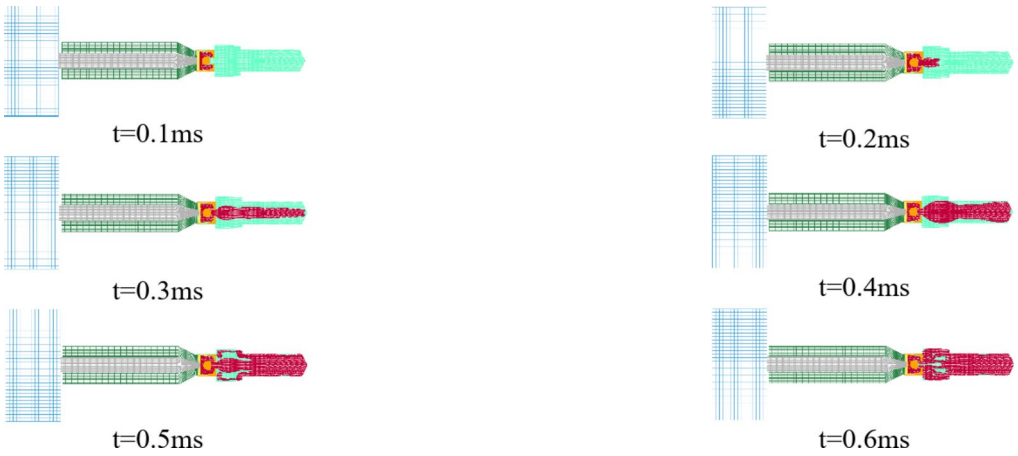

Fig. 16. Firing-ignition response process.

cavity from 500 μs to 600 μs. The pressure variations at the pressure detection point within the cavity are shown in Fig. 17.

As can be observed from the figure, when the combustion products enter the cartridge case through the fire hole, they reach the sensor installation part of the pressure - measuring tooling section within 400 μs. At this point, the pressure value starts to increase, marking the pressure initiation time. The pressure reaches a peak of approximately 16.9 MPa around 500 μs. The time interval from the pressure initiation time to the peak arrival time is about 100 μs.

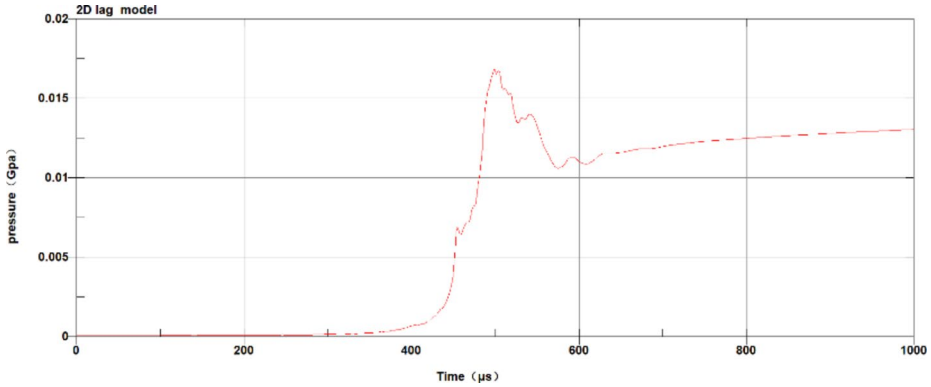

Fig. 17. Pressure-time curve at the monitoring point.

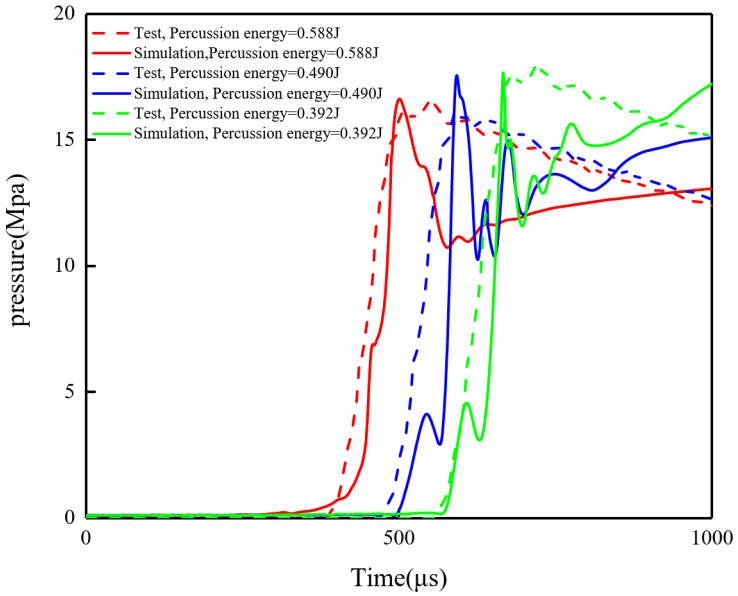

Fig. 18. Comparison of pressure response curves between simulation results and experimental results under different percussion energy.

	Time to pressure initiation/μs			Peak pressure/MPa			Time to peak/μs		
Percussion energy/J	Test data	Simulation results	Error	Test data	Simulation results	Error	Test data	Simulation results	Error
0.588	574.00	579.00	0.87%	17.91	17.67	1.34%	718.00	666.00	7.24%
0.490	488.00	506.00	3.69%	16.02	17.56	9.61%	588.00	592.00	0.68%
0.392	373.70	400.00	7.04%	16.30	16.90	3.68%	522.00	500.00	4.21%

Table 7. Comparison between test data and simulation results.

Finite element model verification of firearm firing-ignition process.

The p - t curves of the experimental results and the simulation results under different percussion energies are compared, as shown in Fig. 18. Table 7 presents several pressure characteristic parameters, including the time to pressure initiation, the time to peak, and the peak pressure, for both the experimental and simulation results.

As can be observed from Fig. 18, when comparing the pressure response curves of the simulation and the test, the trends of pressure initiation and peak arrival are fundamentally consistent. The data presented in Table 7 indicate that the relative errors remained consistently below 10%. This current simulation has the potential to provide significant support for subsequent analyses of hangfire failure.

Influence factors	Data value
percussion energy	[0.392 J,0.539 J]
Interlocking gap	[0.00 mm,0.35 mm]
Charge surface height	[0.46 mm,0.66 mm]
Anvil height	[1.46 mm,1.66 mm]

Table 8. Data ranges of different factors.

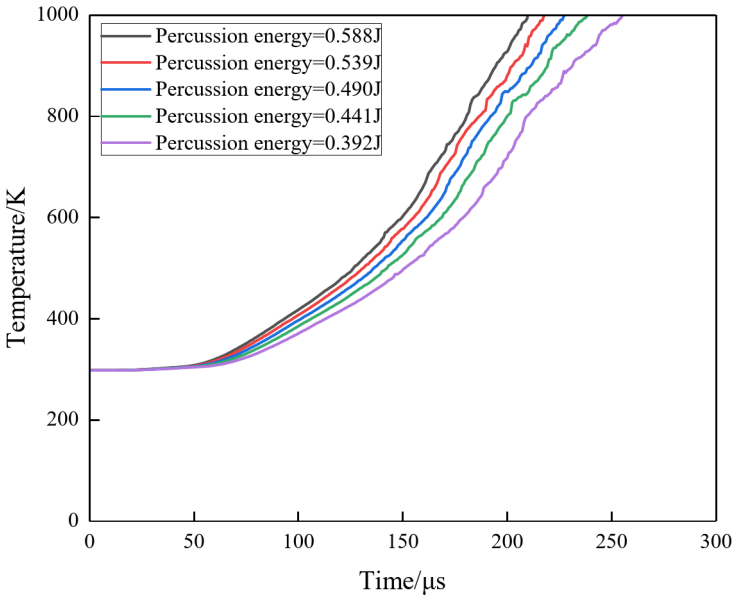

Fig. 19. The influence of percussion energy on the temperature response of primer mixture.

Failure boundary analysis

Single-factor failure boundary and failure mechanism analysis.

In this study, four influencing factors were selected, namely percussion energy, interlocking gap, charge surface height, and anvil height. The control - variable method was employed to analyze the temperature response of the primer mixture and the pressure response within the cartridge cavity. The ranges of these four factors are presented in Table 8. The firing system of a small-caliber automatic rifle is used as an example to illustrate the scenario.

Failure boundary analysis of the percussion energy

The energy generated when the hammer strikes the primer can be considered equivalent to that of a drop - hammer with a specific mass and velocity. In this study, a 250 - g drop - hammer was utilized for calculations. By altering the falling height of the drop - hammer, the percussion energy was regulated within the range of 0.392–0.539 J. Subsequently, the impact of the percussion energy on the temperature response of the primer mixture and the output gas - pressure response of the firearm firing - ignition system was investigated. The corresponding results are presented in Figs. 19 and 20, respectively.

Figures 19 and 20 demonstrate that as the percussion energy declines, the temperature - rising rate of the primer mixture decreases. This leads to an extended period for the temperature to reach the ignition temperature and an increase in the time to pressure initiation. Based on the failure criterion, the critical point for the upper failure boundary was identified as (0.42 J, 550 μs). Consequently, 0.42 J was established as the lower boundary. The safety zone was located to the right of this critical point.

Upon the impact of the firing pin, the primer mixture generates a plastic stress wave, which induces significant plastic deformation within the mixture. During this process, the impact energy is converted into internal energy via the plastic work - heat transformation mechanism, causing the temperature of the primer mixture to rise[32].

As the percussion energy decreases, the impact energy of the firing pin reduces, causing the amplitude of the plastic stress wave to decline. Consequently, both plastic deformation and the conversion of plastic work into heat gradually weaken. This reduction results in a lower heating rate of the primer mixture. The resulting delay restricts the formation of high - temperature zones and hotspots in the extrusion area, leading to a decrease in the combustion rate of the primer mixture.

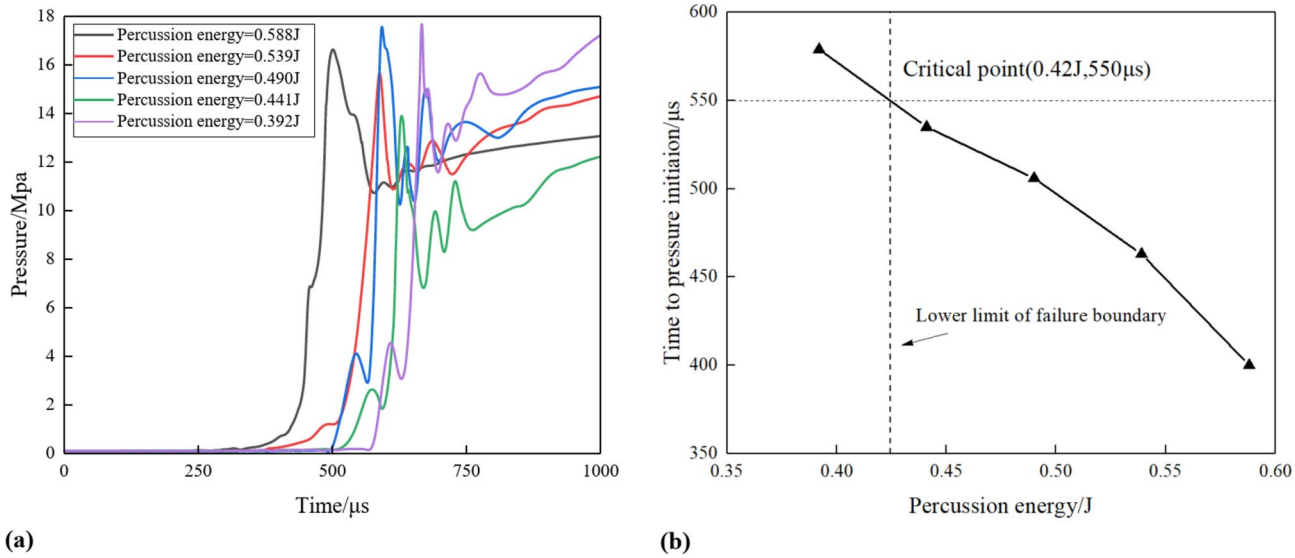

Fig. 20. The influence of percussion energy on gas pressure response.(**a**) Variation curves of the gas pressure at different percussion energy, (**b**). The failure boundary of the percussion energy

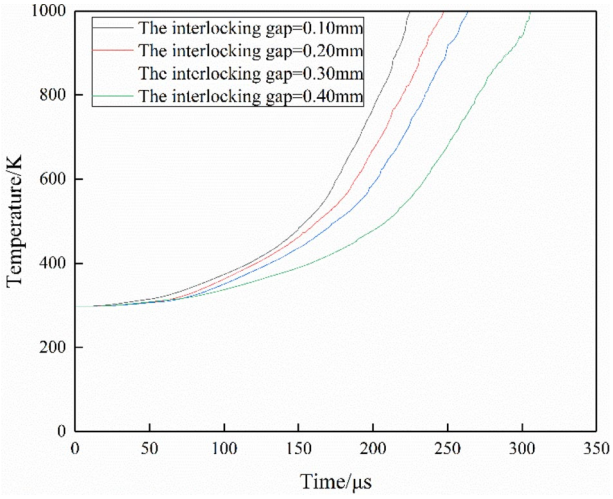

Fig. 21. Variations of the temperature response of the primer mixture at different interlocking gaps.

Failure boundary analysis of the interlocking gap

To explore the impacts of the interlocking gap on the temperature response of the primer mixture and the subsequent gas - pressure response within the firearm's firing - ignition system, the interlocking gap was adjusted within the range of 0.10 mm to 0.40 mm. The corresponding effects are vividly depicted in Figs. 21 and 22, respectively.

As shown in Figs. 21 and 22, as the interlocking gap increases, the temperature of the primer mixture rises at a slower rate. This leads to a delay in the temperature reaching the ignition temperature of the primer mixture. Concurrently, the time needed for pressure initiation also increases. Based on the failure criterion, the critical point for the upper failure boundary was identified as (0.39 mm, 550 μs), and 0.39 mm was determined as the upper limit of the failure boundary. The safety zone is located to the left of this critical point.

When the hammer strikes, as the interlocking gap increases, the effective displacement of the firing pin decreases. Consequently, the loss of percussion energy increases, and the efficiency of energy transfer and conversion into percussion energy declines. As a result, the insufficient energy dissipation impedes the formation of energetic particles required for hotspot creation, thereby reducing the combustion reaction rate of the primer mixture.

Failure boundary analysis of the charge surface height

The height of the charge surface directly affects the dosage of the primer mixture. To explore the influence of the charge - surface height on the temperature response of the primer mixture and the subsequent gas - pressure

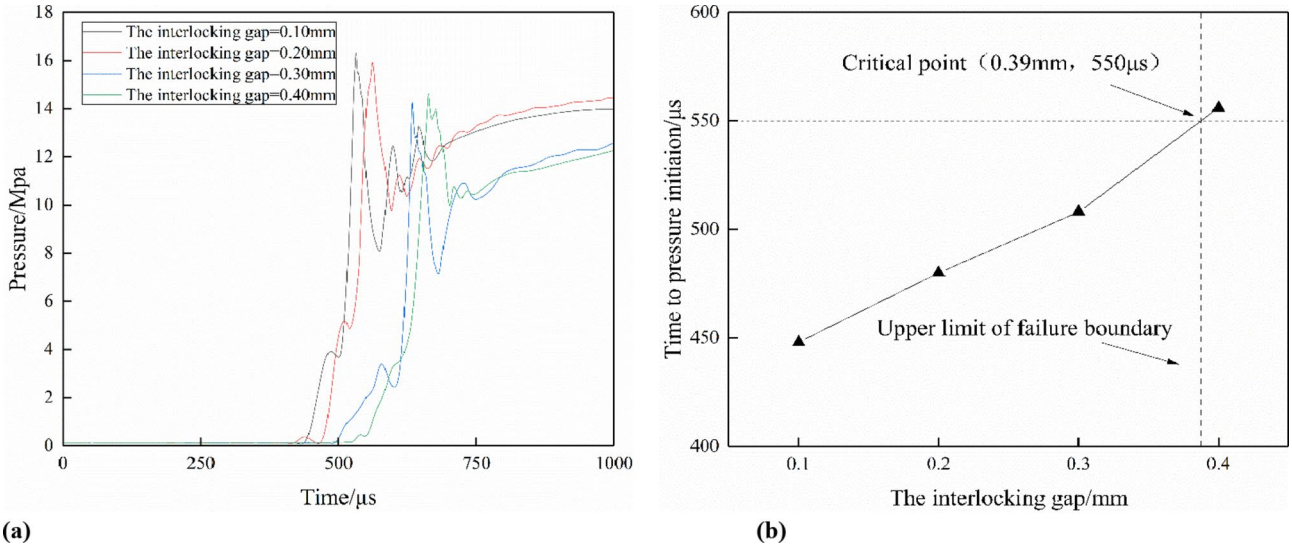

Fig. 22. Effects of the interlocking gap on gas pressure response in the cartridge cavity.(**a**) Variation curves of the gas pressure at different interlocking gaps, (**b**) The failure boundary of the interlocking gap

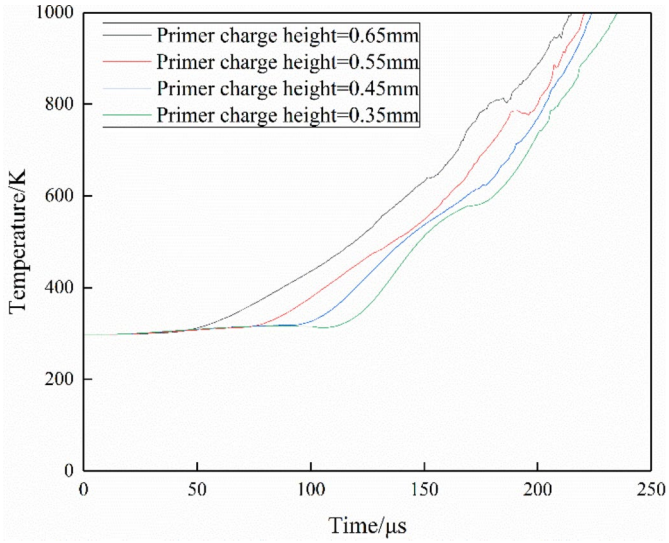

Fig. 23. Effects of the charge surface height on the temperature response of the primer mixture.

response of the firearm's firing - ignition system, the charge - surface height was adjusted within the range of 0.35 mm to 0.65 mm. The corresponding impacts are shown in Figs. 23 and 24, respectively.

As shown in Figs. 23 and 24, as the charge - surface height decreases, the rate of temperature rise in the primer mixture slows down. As a result, it takes longer for the temperature to reach the ignition point of the primer mixture, which in turn leads to an increase in the time to pressure initiation.

Based on the failure judgment criterion, the critical point for the lower failure boundary was determined to be (0.38 mm, 550 μs), and 0.38 mm was set as the lower limit of the failure boundary. The safety zone is located to the right of this critical point.

Based on the hotspot theory, a decrease in the charge - surface height causes non - homogeneity and non - continuity within the propellant grain. This results in a random reduction in the local plastic deformation of the propellant grain[26]. As a consequence, the heat accumulation converted from plastic work is reduced, which in turn lowers both the probability and the number of hotspots. Therefore, the combustion reaction rate of the propellant declines.

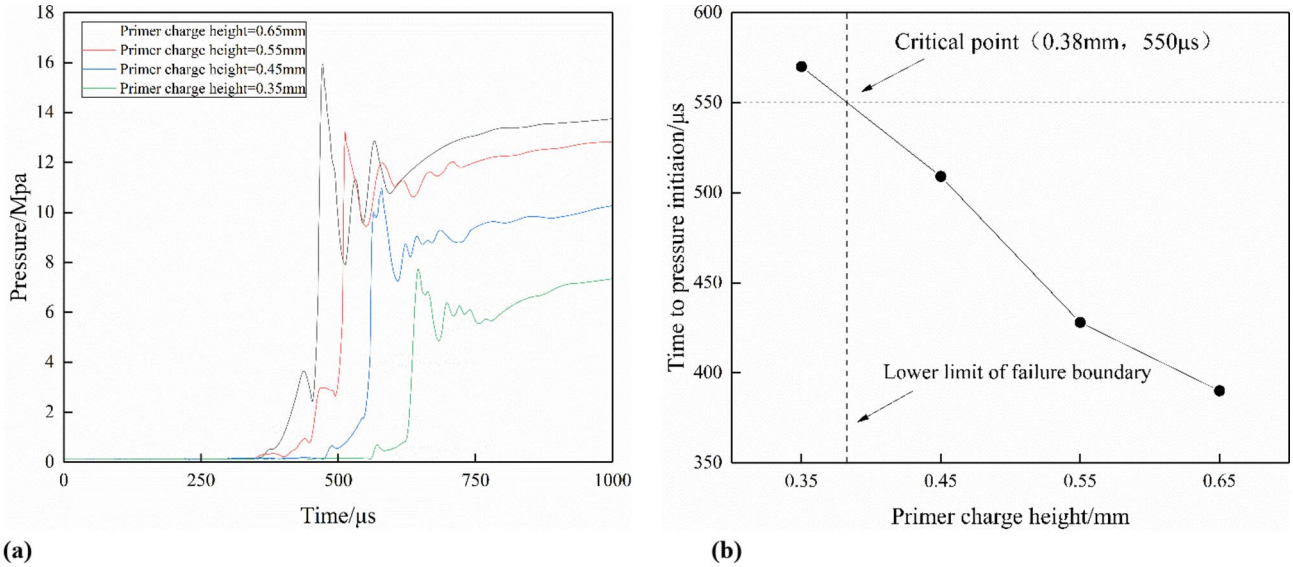

Fig. 24. Effects of the charge surface height on gas pressure response in the cartridge cavity.(**a**) Variation curves of the gas pressure at the charge surface height, (**b**). The failure boundary of the charge surface height

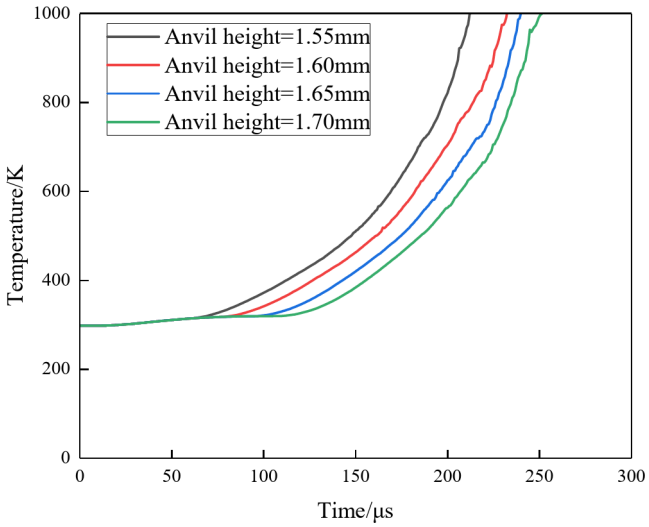

Fig. 25. Effects of the anvil height on the temperature response of the primer mixture.

Failure boundary analysis of the anvil height

To investigate the influence of the anvil height on the temperature response of the primer mixture and the subsequent gas - pressure response within the firearm's firing - ignition system, the anvil height was adjusted within the range of 1.55 mm to 1.70 mm. The corresponding effects are shown in Figs. 25 and 26, respectively.

As shown in Figs. 25 and 26, as the anvil height increases, the heating rate of the primer mixture decreases. This leads to a delay in the temperature reaching the firing temperature of the primer mixture and an extension of the time required for pressure initiation.

Based on the failure judgment criterion, the critical point for the upper failure boundary was identified as (1.69 mm, 550 μs), and 1.69 mm was set as the upper limit of the failure boundary. The safety zone is located to the left of this critical point.

As the anvil height increases, the distance between the anvil and the primer mixture grows. As a result, after the primer mixture undergoes plastic deformation, its contact with the anvil is limited. Owing to friction and shear mechanisms, the formation rate of local hotspots within the deformation layer slows down, which in turn reduces the reaction rate of the primer mixture.

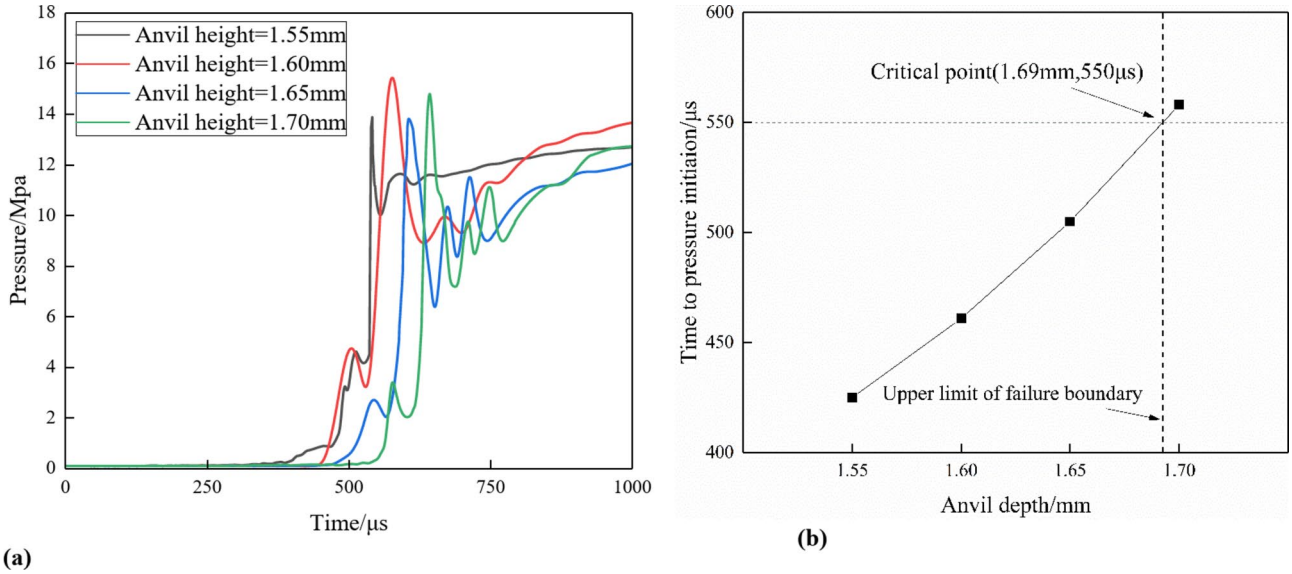

Fig. 26. Effects of the anvil height on gas pressure response in the cartridge cavity.(**a**). Variation curves of the gas pressure at different anvil heights, (**b**). The failure boundary of the anvil height

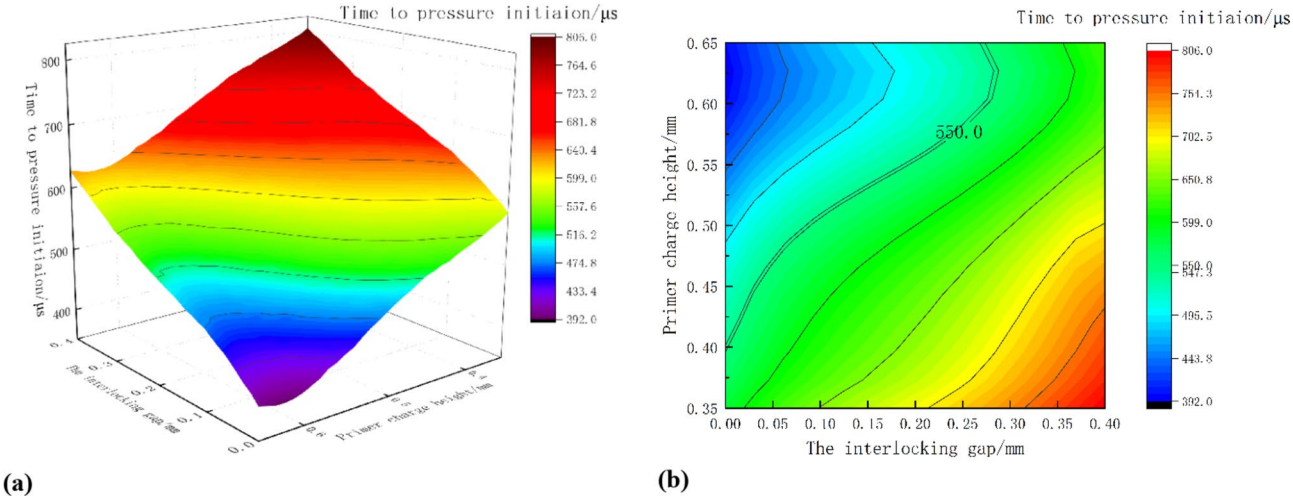

Fig. 27. Coupling influence rules of the interlocking gap and the charge surface height on the time to pressure initiation. (**a**) Coupling effect of the interlocking gap and the charge surface height on the time to pressure initiation, (**b**) Failure boundary under the coupling action of the interlocking gap and the charge surface height

Hangfire failure mechanism under two-factor coupling action

The optimal Latin hypercube experimental design method can strike a balance between the uniformity of sample distribution and the accuracy of model fitting, thus effectively supporting the quantitative analysis of multi-factor coupling[33]. In this study, at a specific falling height, three influencing factors were chosen: the interlocking gap, the charge surface height, and the anvil height. The optimal Latin hypercube experimental design method was employed to analyze the hangfire fault boundary under the coupling of any two factors. The results are presented in Figs. 27, 28 and 29.

In Fig. 27a, when the interlocking gap ranges from 0 to 0.4 mm and the charge surface height is between 0.35 and 0.65 mm, the three - dimensional surface plot of the interlocking gap, charge surface height, and time to pressure initiation shows distinct upward trends in the increasing directions of the charge surface height and the time to pressure initiation. The variation is more gradual along the interlocking gap direction. The time to pressure initiation ranges from 392 μs to 806 μs.

As the interlocking gap increases, the percussion energy declines, leading to a decrease in the ignition energy converted from the percussion energy. On the contrary, a reduction in the charge surface height directly diminishes both the number of hotspots formed and the combustion reaction rate of the primer mixture. Consequently, the time to pressure initiation shows more pronounced variations.

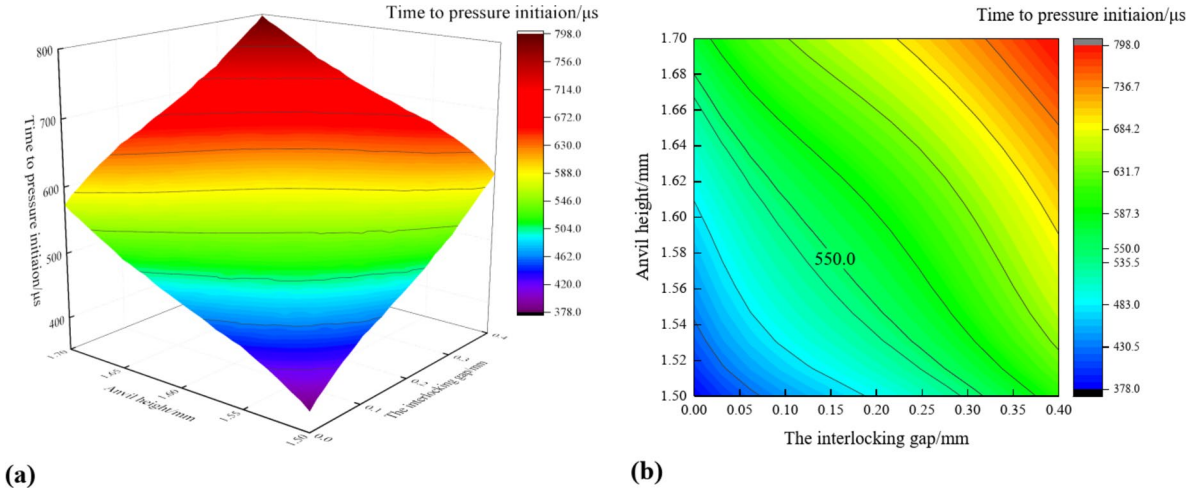

Fig. 28. Coupling influence rules of the interlocking gap and the anvil height on the time to pressure initiation, (**a**) Coupling effect of the interlocking gap and the anvil height on the time to pressure initiation, (**b**) Failure boundary under the coupling action of the interlocking gap and the anvil height

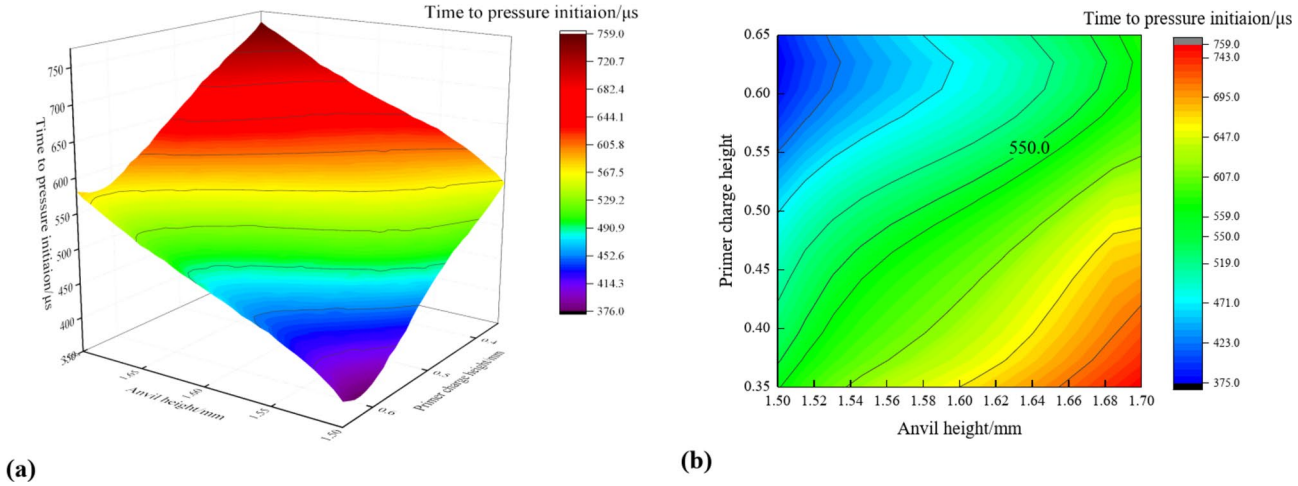

Fig. 29. Coupling influence rules of the anvil height and the charge surface height on the time to pressure initiation. (**a**) Coupling effect of the anvil height and the charge surface height on the time to pressure initiation, (**b**). Failure boundary under the coupling action of the anvil height and the charge surface height

In Fig. 27b, under the strong coupling effect of the interlocking gap and the charge surface height, the critical threshold of the interlocking gap associated with hangfire failure decreases, whereas the critical value of the charge surface height increases. The safety zone is located above the failure boundary.

In Fig. 28a, when the anvil height ranges from 1.50 to 1.70 mm and the interlocking gap ranges from 0 to 0.4 mm, the three - dimensional surface plot of the anvil height, interlocking gap, and time to pressure initiation reveals a slight upward trend in the increasing directions of the anvil height and the time to pressure initiation. The variation is less significant compared to that along the interlocking gap direction. The time to pressure initiation ranges from 378 μs to 798 μs.

As the interlocking gap increases, the ignition energy converted from the percussion energy declines. Meanwhile, an increase in the anvil height delays the moment when the primer mixture is subjected to pinning action. As a result, the proportion of percussion energy used for hotspot formation decreases, leading to more pronounced variations in the time to pressure initiation.

Moreover, in Fig. 28b, both the critical threshold of the interlocking gap associated with hangfire failure and that of the anvil height decline. The safety zone is located below the failure boundary.

In Fig. 29a, when the anvil height ranges from 1.50 mm to 1.70 mm and the charge surface height ranges from 0.35 mm to 0.65 mm, the three - dimensional relationship among the anvil height, charge surface height, and time to pressure initiation shows a distinct upward trend in the increasing directions of the charge surface height and the time to pressure initiation. The variation is less significant compared with that along the anvil height direction. The time to pressure initiation ranges from 376 μs to 759 μs.

·	Influence factor	Influence mechanism
Single-factor	Percussion energy	As the percussion energy declines, the impact energy of the firing pin decreases, which in turn reduces the amplitude of the plastic stress wave. As a consequence, both plastic deformation and the conversion of plastic work into heat gradually weaken. This reduction leads to a slower heating rate of the primer mixture, causing a delay in the temperature reaching the ignition temperature. This delay restricts the formation of high - temperature zones and hotspots in the extrusion area, resulting in a drop in the combustion rate of the primer mixture and an extended time to pressure initiation.
	Interlocking gap	As the interlocking gap increases, when the firing pin is impacted by the hammer, its effective displacement decreases. As a result, the loss of percussion energy increases, and the efficiency of energy transfer and conversion into percussion energy declines. This causes a gradual reduction in both plastic deformation and the conversion of energy through plastic work, leading to a delay in the time it takes to heat up to the ignition temperature. Consequently, insufficient energy dissipation impedes the formation of energetic particles required for hotspot creation, thereby reducing the combustion reaction rate of the primer mixture and, in turn, increasing the time needed for pressure initiation.
	Primer charge height	Based on the hotspot theory, a decrease in the charge surface height causes non - homogeneity and non - continuity within the propellant grain, leading to a random decrease in the local plastic deformation of the propellant grain. This reduction in the heat accumulated from plastic work lowers both the probability and the number of hotspots. As a result, the time it takes to heat the primer mixture to the firing temperature is prolonged. Subsequently, the combustion reaction rate of the primer mixture decreases, and the time needed for pressure initiation increases.
	Anvil height	When the primer mixture is deformed by impact energy, it is subjected to the pinning action of the anvil after this plastic deformation, which leads to the formation of hotspots beneath the pinned region. As the anvil height increases, the distance between the anvil and the primer mixture grows. As a result, the contact between the primer mixture and the anvil is limited after the plastic deformation. Owing to friction and shear mechanisms, the formation rate of local hotspots within the deformation layer slows down, delaying the time it takes to heat the primer mixture to its firing temperature. Meanwhile, the reaction rate of the primer mixture decreases, which in turn extends the time needed for pressure initiation.
Two-factor coupling	Interlocking gap and primer charge height	As the interlocking gap increases, the percussion energy declines, leading to less plastic deformation of the primer mixture. Meanwhile, the rate of temperature rise induced by the plastic work within the primer mixture slows down, delaying the formation of hotspots. On the contrary, a reduction in the charge surface height directly weakens the plastic deformation of the primer mixture. As a consequence, the plastic deformation zone narrows, which reduces both the number of hotspots formed and the combustion reaction rate of the primer mixture. Consequently, the time to pressure initiation shows more pronounced variations.
	Interlocking gap and anvil height	As the interlocking gap increases, the percussion energy declines, subjecting the primer mixture to a lower load. As a result, the mass points within the primer mixture undergo less plastic deformation under the action of the stress wave. A smaller proportion of the percussion energy is converted into energy for volume - deformation work within the primer mixture, leading to a slower rate of temperature rise due to the heat conversion from plastic work. Meanwhile, an increase in the anvil height delays the moment when the primer mixture is subjected to pinning action. The greater distance between the primer mixture and the anvil means that more plastic deformation is required for the primer mixture to come into contact with the anvil. Consequently, the proportion of percussion energy used for hotspot formation decreases, which reduces the combustion reaction rate within the primer mixture. As a consequence, the time to pressure initiation shows more pronounced variations.
	Anvil height and primer charge height	A change in the anvil height can lead to increased energy dissipation and affect the accumulation of hotspots. Likewise, variations in the charge surface height affect the amount of the primer mixture. As a result, the number of hotspots is impacted, and the combustion reaction rate within the primer mixture decreases. Consequently, the time to pressure initiation shows more pronounced variations.

Table 9. The influence mechanism of different influence factors.

A change in the anvil height can lead to an increase in energy dissipation and affect the accumulation of hotspots. Likewise, variations in the charge surface height affect the dosage of the primer mixture, which in turn impacts the number of hotspots and reduces the combustion reaction rate within the primer mixture. As a result, the time to pressure initiation shows more pronounced variations.

Moreover, in Fig. 29 (b), under the coupling effect of the anvil height and the charge surface height, the critical thresholds of both the interlocking gap and the anvil height associated with hangfire failure decline. The safety zone is located above the failure boundary.

The influence mechanisms of various factors on hangfire failure are systematically summarized in Table 9, which presents::

In this paper, the research on the factors contributing to hotspot formation and the insufficiency of percussion energy, which can lead to hangfire faults, aligns with the current theory. Nevertheless, this paper uncovers the mechanism of hangfire failures from the perspective of the transfer of percussion energy to ignition energy. This discovery offers a new avenue for predicting hangfire failures and holds certain significance in reducing the failure rate of the firing-ignition system.

Conclusions

Taking a small-caliber automatic rifle as a model, this study investigated four crucial influencing factors: percussion energy, the interlocking gap, the primer charge surface height, and the anvil height. Subsequently, it analyzed how these factors affect the boundaries of hangfire failures.

(1) When compared with the experimental results, the simulation data showed an error margin of less than 10%, indicating that the established model is reliable in simulating the mechanical firing response process. The control - variable method was employed to simulate the hangfire fault boundary under the influence of a single factor. The percussion energy was set in the range of 0.392–0.539 J, the interlocking gap in the range of 0–0.4 mm, the charge surface height in the range of 0.35–0.55 mm, and the anvil height in the range of 1.55–1.70 mm.

The simulation results reveal that the percussion energy and the charge surface height have lower bounds, which are 0.42 J and 0.38 mm respectively. The interlocking gap and the anvil height have upper limits, which are 0.39 mm and 1.69 mm respectively.

(2) In the small-caliber automatic rifle, increasing the falling height leads to an enhancement of percussion energy. This has a positive impact on the temperature rising rate of the primer mixture and reduces the time to firing initiation. Similarly, decreasing the interlocking gap and the anvil height also yield similar positive effects. Moreover, increasing the primer charge surface height demonstrates comparable favorable influences.

(3) The influence of two - factor coupling on the pressure initiation time and the hangfire fault boundary was investigated. The anvil height was restricted to the range of 1.50 –1.70 mm, the interlocking gap to 0 –0.4 mm, and the charge surface height to 0.35 –0.65 mm.

The results indicate that when the interlocking gap increases and the anvil height rises, the time to pressure initiation shows consistent variation trends. However, the delay is more significant compared to the cases analyzed individually.

(4) The mechanism of hangfire failure entails a reduction in ignition energy during the transmission and conversion of percussion energy. This reduction weakens the plastic deformation of the primer mixture and the conversion of work into heat. As a result, the rate of temperature rise decreases, the growth of hotspots is delayed, the combustion of the primer mixture is reduced, and the time to pressure initiation increases. This chain of events delays hangfire failures.

The findings of this study provide valuable insights into the factors that influence hangfire failures and offer crucial understanding for improving the reliability of firearm firing - ignition systems. However, this study has certain limitations. It only takes into account the influence of different factors on temperature and pressure, with a limited number of indicators. Additionally, it only focuses on the primer mixture. In the next step, the propellant can be included in the research, which will make the study more comprehensive.

Data availability

The datasets used and/or analysed during the current study available from the corresponding author on reasonable request.

Received: 31 October 2024; Accepted: 17 March 2025
Published online: 24 March 2025

References

1. , Z. C. C.,, W. Z. F. &, G. X. X. Design of simulation test device for firing system of firearms. *J. Ordnance Ind. Autom.* **41**, 10–13 (2022). 18.
2. Wei, L. et al. Experimental study on performance of gun propellant coating containing barium nitrate.*J. Ordnance Equipment Eng.*43,238–242 (2022).
3. Zhang, L. K., Zhou, Y. H. & Yu, Y. G. Effect of jet of base bleed igniter on ignition delay time.*J. Ballistics*, 22,8–11 (2010).
4. Courtney, E. et al. Performance testing of lead free primers: blast waves, velocity variations, and environmental testing.*Physics* (2014).
5. Zejun, H. U. et al. Ignition and combustion characteristics of micro-sized aluminum particles in H2O and O2.*Acta Aeronautica ET Astronautica Sinica*,44,248–257 (2023).
6. Xueqin, L. I. A. O. et al. Study on effect of pressure on ignition,combustion and agglomeration characteristics of GAP/CL-20. *J. Propellant Initiators Pyrotechnics*. **2**, 44–48 (2023).
7. Mcbain, A. et al. Laser ignition of CL-20 (hexanitrohexaazaisowurtzitane) cocrystals. *J. Combust. Flame*. **188**, 104–115 (2018).
8. Posey, J. W. et al. Mechanisms of prompt and delayed ignition and combustion of explosively dispersed aluminum powder. *J. Phys. Fluids* (2021).
9. Frost, D. L. & Zhang, F. Nonideal blast waves from heterogeneous explosives. *J. Mater. Sci. Forum*. **465–466**, 421–426 (2004).
10. Li, G. H. et al. Fault simulation analysis of mechanical firing based on fault tree. *J. J. Mach. Des.* **30**, 8–11 (2013).
11. Jing, Y. P. & Yang, Z. Application of finite element method in percussion of firearms.*Mech. Eng. Automation*.3, 48–49 + 52 (2007).
12. Ge, T., Jia, Z. H. & Zhou, K. L. Study on firing process of firing mechanism of a rifle. *J. J. Ballistics*. **2**, 77–80 (2008).
13. Wang, R. et al. Research on the design of A semiconductor laser ignition system. *J. Pyrotechnics*. **2**, 5–8 (2022).
14. Huang, Y. H. Fluid-Structure interaction numerical simulation of solid rocket motor ignition and pressure forming process. *Harbin Eng. Univ.* **001390** (2020).
15. Xie, W. H., Bai, N. D. & Sun, D. Y. Safety problems of dud left in the bore. *J. Ordnance Ind. Autom.* **39**, 93–96 (2020).
16. Wu, F. M. & Chen, J. W. Cartridge retention problem of a new type submachine gun system. *J. J. Ordnance Equip. Eng.* **29**, 10–12 (2008).
17. Zhang, H. Y. Failure analysis of cartridge burst of a certain gatling gun.*J. Gun Launch & Control.*40, 84–89 (2019).
18. Courtney, M. et al. High-speed measurement of firearm primer blast waves. *J. Phys.* (2012).
19. Mei, M. et al. Influence analysis of delayed ignition on dynamic characteristics of internal energy automatic gun. *J. Ordnance Ind. Autom.* **41**, 11–17 (2022).
20. Zhou, Q., Li, Q. & Wang, Z. M. Numerical simulation of influence on projectile posture based on hangfire failure of cluster weapon. *J. J. Projectiles Rockets Missiles Guidance*. **33**, 83–85 (2013).
21. Li, Q. Q., Chen, J. & Liu, S. X. Analysis and inspiration of fault causation for cartridge explosion in a certain type of automatic cannon. *J. J. China Ordnance*. **34**, 5–7 (2013).
22. Yang, J. R. Dynamic analysis of an auto mortar based on the soft recoil technology.*J. Ballistics*.1, 63–67 (2006).
23. Duan, H. et al. Ignition response of NEPE-based propellants under drop weight through experiments and numerical simulation. *J. Polym. Test.* **116** (2022).
24. WEI, Z., Xin, C., Hou, X., Su, Y. & Wang, F. Mechanical–thermal– chemical coupled modeling techniques and numerical simulation methods for the firearm igniting process. *Propellants, Explos., Pyrotech.* **48**, e202200244. https://doi.org/10.1002/prep.202200244 (2023).
25. Zhu, Q. X. et al. WJ 2644 – 2005, General specifications for cartridge primer,2005.
26. Qu, K. P. et al. Impact safety of composition B under thermo-mechanical coupling condition.*Chin. J. Explosive & Propellants*.43, 330–334 (2020).
27. Hao, B., Liu, L. W. & Jiang, Q. Research on calculating parameters of JWL equation of state for explosive based on hybrid algorithm. *J*, engineering blasting.30, 42–48,97 (2024).
28. DING L Z et al. Research on low velocity impact characteristics of particle explosives based on ignition growth model. *J*, pyrotechnics.3, 38–43 (2022).
29. ZHANG, D. J. et al. Calibration and verification of dynamic mechanical properties of High-strength armored steel based on Johnson-Cook constitutive model. *Acta Armamentarii*. **43**, 1966–1976 (2022).
30. Jiang, T., Hu, Z. Y. & Gao, X. Y. Numerical simulation of penetration process of tungsten wire reinforced Copper-Zine composite. *Rare Metal Mater. Eng.* **52**, 1296–1302 (2023).
31. Zhang, S. et al. *A Simulation Test Device for Firearm firing-ignition System. P. Shanxi Province: CN202110249900*September 9 (X, 2022).

32. Jia, X. Z., Wang, Y. S. & Liu, R. P. Test and numerical simulation of explosive impact with rigid target plate. *J. J. Ordnance Eng.* **40**, 212–216 (2019).
33. Zhu, Y. H. *Research on Reliability Control Methods for Firearm Firing Ignition in Special Environments* (North University of China, 2024).

Author contributions

S.Z. (Shuxia Zhang) writing—original draft preparation; S.Z. (Shuxia Zhang) writing—review and editing; Y.L. (Yirui Li) and Z.W. (Zhifang Wei) performed the experiments; J.L. (Jinguo liang) and T.X. (Tantao Xiang) analyzed the data; K.Z. (Kebin Zhang) revised the paper. All authors discussed the results and improved the final text of the paper. All authors have read and agreed to the published version of the manuscript.

Declarations

Competing interests

The authors declare no competing interests.

Additional information

Correspondence and requests for materials should be addressed to S.Z.

Reprints and permissions information is available at www.nature.com/reprints.

Publisher's note Springer Nature remains neutral with regard to jurisdictional claims in published maps and institutional affiliations.

Open Access This article is licensed under a Creative Commons Attribution-NonCommercial-NoDerivatives 4.0 International License, which permits any non-commercial use, sharing, distribution and reproduction in any medium or format, as long as you give appropriate credit to the original author(s) and the source, provide a link to the Creative Commons licence, and indicate if you modified the licensed material. You do not have permission under this licence to share adapted material derived from this article or parts of it. The images or other third party material in this article are included in the article's Creative Commons licence, unless indicated otherwise in a credit line to the material. If material is not included in the article's Creative Commons licence and your intended use is not permitted by statutory regulation or exceeds the permitted use, you will need to obtain permission directly from the copyright holder. To view a copy of this licence, visit http://creativecommons.org/licenses/by-nc-nd/4.0/.

© The Author(s) 2025